LETTERS

Synthetic lethal screen identification of chemosensitizer loci in cancer cells

Angelique W. Whitehurst[1], Brian O. Bodemann[1], Jessica Cardenas[1], Deborah Ferguson[2], Luc Girard[3], Michael Peyton[3], John D. Minna[3,4], Carolyn Michnoff[5], Weihua Hao[5], Michael G. Roth[5], Xian-Jin Xie[4,6] & Michael A. White[1,4]

Abundant evidence suggests that a unifying principle governing the molecular pathology of cancer is the co-dependent aberrant regulation of core machinery driving proliferation and suppressing apoptosis[1]. Anomalous proteins engaged in support of this tumorigenic regulatory environment most probably represent optimal intervention targets in a heterogeneous population of cancer cells. The advent of RNA-mediated interference (RNAi)-based functional genomics provides the opportunity to derive unbiased comprehensive collections of validated gene targets supporting critical biological systems outside the framework of preconceived notions of mechanistic relationships. We have combined a high-throughput cell-based one-well/one-gene screening platform with a genome-wide synthetic library of chemically synthesized small interfering RNAs for systematic interrogation of the molecular underpinnings of cancer cell chemoresponsiveness. NCI-H1155, a human non-small-cell lung cancer line, was employed in a paclitaxel-dependent synthetic lethal screen designed to identify gene targets that specifically reduce cell viability in the presence of otherwise sublethal concentrations of paclitaxel. Using a stringent objective statistical algorithm to reduce false discovery rates below 5%, we isolated a panel of 87 genes that represent major focal points of the autonomous response of cancer cells to the abrogation of microtubule dynamics. Here we show that several of these targets sensitize lung cancer cells to paclitaxel concentrations 1,000-fold lower than otherwise required for a significant response, and we identify mechanistic relationships between cancer-associated aberrant gene expression programmes and the basic cellular machinery required for robust mitotic progression.

Paclitaxel and related taxanes are routinely used in the treatment of non-small-cell lung cancer (NSCLC) and other epithelial malignancies. Although objective responses and survival benefits are seen, complete responses are uncommon. Half-maximal inhibitory concentrations (IC_{50} values) of Paclitaxel in a panel of 29 human primary lung-tumour-derived cell lines spanned a wide range of concentrations, from 1 nM to more than 1 mM (M.P., L.G. and J.D.M., unpublished observations). From this panel, we selected the NSCLC line NCI-H1155 for a genome-wide paclitaxel synthetic-lethal screen, given the IC_{50} (about 50 nM) for this line, which is tenfold that observed for many other lines with similar proliferation rates. A high-efficiency, high-throughput short interfering RNA (siRNA) reverse transfection protocol was designed on the basis of our observations that transient trypsin-mediated suspension of adherent cultures markedly enhances the cellular uptake of liposome/nucleic acid particles[2,3] (Supplementary Fig. 1a).

We employed a library of 84,508 siRNAs corresponding to four unique siRNA duplexes, targeting each of 21,127 unique human genes arrayed in a one-gene–one-well format on 96-well microtitre plates (Supplementary Table 1). Transfections were performed in sextuplicate for triplicate analysis in the presence and the absence of paclitaxel (Supplementary Fig. 1b). A 48-h exposure to 10 nM paclitaxel was used as an otherwise innocuous dose that was in range of a significant response at a tenfold higher drug concentration (Supplementary Fig. 1c). Cell viability was measured using ATP concentration, and raw values were normalized to internal reference control samples on each plate to permit plate-to-plate comparisons[4] (Supplementary Table 1 and Supplementary Fig. 1f). Each siRNA pool was assigned a viability ratio calculated as mean viability in paclitaxel divided by mean viability in the absence of drug ($mean_{paclitaxel}/mean_{carrier}$) (Supplementary Fig. 1d).

An objective protocol for the selection of significant 'hits' was derived to combine reproducibility of testing with magnitude of response (Supplementary Fig. 1e, and Methods described therein). First, we set a 5% false discovery rate (FDR) by using two-sample *t*-tests from the triplicate analysis together with *P*-value corrections for the multiplicity of testing[5–8] (Supplementary Table 2). Second, we selected all samples that both satisfied a 5% FDR and were present in the 2.5-centile rank of the viability ratios (Supplementary Table 3 and Supplementary Fig. 1e). A set of 87 candidate paclitaxel-sensitizer loci, defined as 'high-confidence hits', was identified that satisfied these criteria (Table 1). Retests of a subset of these candidates with independently synthesized siRNA pools reproduced a significant response to 10 nM paclitaxel (Fig. 1a).

A 5% FDR is a highly stringent cut-off that may produce many false negatives. Nonetheless, this cut off returned many candidates with overlapping functional relationships, including macromolecular complexes, receptor–ligand pairs, and products of related aberrant gene-expression programmes (Table 1, Fig. 1b–e, and Supplementary Table 4). Most striking was the presence of a large group of core components of the proteasome (Fig. 1b), consistent with numerous empirical observations of enhanced sensitivity to paclitaxel in cancer cells after proteasome inhibition. Multiple targets encoding proteins involved in the dynamics and function of microtubules were also isolated[9] (Table 1). Relaxing the FDR to 10% returned most of the known main components of the γ-tubulin ring complex (γ-TuRC), a central element of the microtubule organizing centres that nucleate the formation of the mitotic spindle[10] (Fig. 1c, and Supplementary Table 4). Isolation of these components is evocative of a successful primary screen, because the mitotic spindle apparatus is exquisitely sensitive to the inhibition of microtubule dynamics by paclitaxel and is probably the biologically relevant drug target in cancer cells[11]. The probabilities of this extent of enrichment of proteasome subunits and of γ-TuRC subunits by random chance are 1 in 10^{10} ($P \leq 0.0000000001$)

[1]Department of Cell Biology, [2]Reata Pharmaceuticals, [3]Hamon Center for Therapeutic Oncology Research, [4]Simmons Cancer Center, [5]Department of Biochemistry, and [6]Center for Biostatistics and Clinical Science, University of Texas Southwestern Medical Center, Dallas, Texas 75390, USA.

Table 1 | High-confidence hit list

Symbol	Comments; motifs	Symbol	Comments; motifs
Proteasome		**Transcription**	
PSMA6	Proteasome subunit	RP9	ZnF_C2HC
PSMA7	Proteasome subunit	ZFPM1	ZnF_C2H2(x9)
PSMA8 (MGC26605)	Proteasome subunit	ZNF503	ZnF_C2H2
PSMB1	Proteasome subunit	ZNF585A	KRAB; ZnF_C2H2(x21)
PSMC3	Proteasome subunit	C11ORF30	ENT
PSMD1	Proteasome subunit	TRIM15	RING, BBOX, PRY, SPRY
PSMD3	Proteasome subunit		
		Translation	
Microtubule-related		RARSL	Arginyl-tRNA synthetase-like; Arg_S Core, tRNA-synt_1d_C
TUBGCP2	γ-TURC subunit; Spc97_Spc98	LOC390876	Similar to 60S ribosomal protein L35; coiled-coil
TUBA8	α-Tubulin	LOC388568	Similar to ribosomal protein S15 isoform
DNHD1 (FLJ32752)	Dynein heavy-chain subunit	SYMPK	
DNAH10 (FLJ43808)	Dynein heavy-chain subunit	SYNCRIP	RRM
TBL1Y	Transducin (β)-like 1Y-linked; LisH, WD40	BCDIN3 (FLJ20257)	Bin3, PrmA
MPP7	MAGUK family; L27, PDZ_signalling, SH3, GMPK	LOC144233	Bin3
Post-translational modification		**Channel**	
FBXO18	FBOX, UvrD-helicase	ATP6V0D2	Lysosomal H$^+$ transporter; vATP-synt_AC39
RAI17	Similar to PIAS; zf-MIZ	SLC34A3	Solute carrier; Na_Pi_cotrans
RNF151	RING		
LOC389822 (DKFZp434E1818)	Transmembrane, RING	**Membrane protein**	
LOC401506 (new LOC648245)	RING	BEAN	Transmembrane, basic domain
HS6ST2	Heparan sulphotransferase	LRRTM1	LLRNT, LRR (×9), transmembrane
GAL3ST4	Galactose sulphotransferase	MGC31967	Transmembrane, C-C
MGC4655	Galactosyl_T	TMC05 (MGC35118)	Transmembrane, C-C
Cell adhesion/ECM receptor		**Other**	
PAPLN	Proteoglycan-like sulphated glycoprotein; TSP1.KU, IGcam	PDDC1 (FLJ34283)	GATase1_Hsp31_like
KIAA1920	Similar to chondroitin sulphate proteoglycan 4	C14ORF148	Predicted NADP oxidoreductase; P5CR
LRFN5	LRR, COG4886, IGcam, transmembrane	CWF19L2	Similar to CWF19; CwfJ_C_1, CwfJ_C_2
MGC33424	IG_FLMN, CAP10, KDEL	PRICKLE1	Planar cell polarity, nuclear receptor for REST; PET, LIM (×3)
C1QTNF3	C1q	CA10	Carbonic anhydrase; alpha_CARP_X_XI_like
ITIH5	VIT, vWA_interalpha_trypsin_inhibitor	FAM14B	Similar to ISG12, aIFN-inducible; Ifi-6-16
IGSF21 (MGC15730)	IGcam	TIP39	PTHR2 ligand
		HSN2	Hereditary sensory neuropathy locus
Gametogenesis-associated/cancer testis antigens		**Unknown**	
ACRBP	sp32, Kazal	NOD9	NACHT, LRR
FMR1NB	Transmembrane (×2), basic domain	F25965	
STARD6	START	LOC348262	
FSIP1	CC (×2)	C8orf33 (FLJ20989)	
		ANKRD41 (FLJ39369)	Ankyrin domains (ANK)
Receptor		CCDC38 (FLJ40089)	Coiled-coil
NTNG2	LamNT, EGF_Lam	C2orf33 (GL004)	DUF800
GPR144	PTX, GPS, 7transmembrane_2	NLF1 (LOC145741)	NF-κB target gene
PDCL	Similar to phosducin	BU077088 (LOC284409)	Transmembrane
		BX103302 (LOC284931)	
Ras family		LOC340109	
FGD4	FYVE, RhoGEF and PH-domain-containing 4	C21orf111 (LOC388830)	
FLJ32810	Rho_GAP, SH3	LOC400236	
SIPA1L2	Rap_GAP, PDZ_signalling	LOC400861	
RAB9A	RAB	LOC55924	
SYT13	Rab effector; C2	LOC56181	DUF729
		MGC10701	
		MGC15634	
		LOC56390 (LOC388497)	
		LOC257396	

and 1 in 3×10^9 (γ-TuRC, $P \le 0.000000003$), respectively, as calculated by hypergeometric distribution analysis.

A surprising observation was the enrichment of genes, the expression of which is normally restricted to the testis. Four of these are known to encode tumour antigens that are markedly upregulated in many tumour types including NSCLC, breast cancer and melanoma (Fig. 1e; $P \le 0.003$ (hypergeometric distribution)). The restricted expression pattern and immunogenicity of cancer/testis antigens (CT antigens) has driven forward efforts for their use in cancer vaccines even in the absence of functional information[12]. Their identification in this screen suggests the obligatory participation of some CT antigens in aberrant cancer-cell regulatory programmes.

To probe the extent of chemosensitization that can be conferred by target gene depletion, a panel representing six functionally diverse groups from the 'high-confidence' hit list was selected. This panel included the following: CT-antigen ACRBP; the proteasome subunit PSMA6; the γ-TuRC protein TUBGCP2; a heparin sulphate transferase, HS6ST2, with significantly enriched expression in lung tumour tissue compared with normal lung (L.G. and J.D.M., unpublished observations); a vacuolar ATPase subunit, ATP6V0D2, expressed from a locus amplified in several lung cancer lines; and FGD4, a CDC42 activator. As controls for 'off-target' siRNA phenomena, we verified that each siRNA pool resulted in target gene knockdown, that at least two single siRNAs would recapitulate the phenotype

when tried separately, and that distinct pools of four more independent siRNAs against each gene also resulted in target knockdown and paclitaxel sensitization (Supplementary Fig. 2a–d).

We next examined the consequence of target depletion on responses to a broad range of concentrations of paclitaxel, vinorelbine and gemcitabine. Paclitaxel and vinorelbine impair mitotic spindle assembly through independent mechanisms that suppress microtubule dynamics[11]. In contrast, gemcitabine induces replication-stress-dependent apoptosis through DNA chain termination[13]. Several targets displayed significant collaboration with paclitaxel concentrations 1,000-fold below that used for the primary screen (Fig. 2a). Exposure to paclitaxel for a further 24–48 h magnified these differences: some groups responded to paclitaxel concentrations 10,000-fold lower than otherwise required (Fig. 2d). Cell survival curves and colony assays suggest that the decrease in cell number is a consequence of cell death rather than a transient delay in proliferation (Supplementary Fig. 3a, b). Some targets also significantly enhanced sensitivity to vinorelbine but, for the most part, only at concentrations at which vinorelbine alone detectably impaired cell viability (Fig. 2b). In contrast, target depletion had no remarkable

consequence on the maximally effective concentration of gemcitabine in H1155 cells, although the non-responding cell population was decreased or eliminated in all cases (Fig. 2c).

The apparent synergy that we observed between target depletion and paclitaxel, in comparison with other chemotherapeutic agents, suggests that genome-wide chemosensitizer screens return molecular components closely related to the mode of action of a particular drug. To test this directly, we examined the consequence of target depletion on the morphology of the mitotic spindle[14]. Depletion of FGD4 resulted in a significant accumulation of otherwise normal-appearing mitotic figures in the absence of paclitaxel, indicating that this protein may be required for support of mitotic progression (Supplementary Fig. 4). Depletion of ACRBP and TUBGCP2, although not detectably affecting mitosis in the absence of drug, resulted in a marked accumulation of multipolar spindles in the presence of 10 nM paclitaxel (Fig. 3a, and Supplementary Fig. 5b). Multipolar spindle accumulation is typical after exposure to higher doses of paclitaxel in H1155 cells as well as in other cancer cell types[9,11] (data not shown). Simultaneous depletion of MAD2, an obligate component of the spindle assembly checkpoint[14], reversed the accumulation of mitotic figures with the concomitant appearance
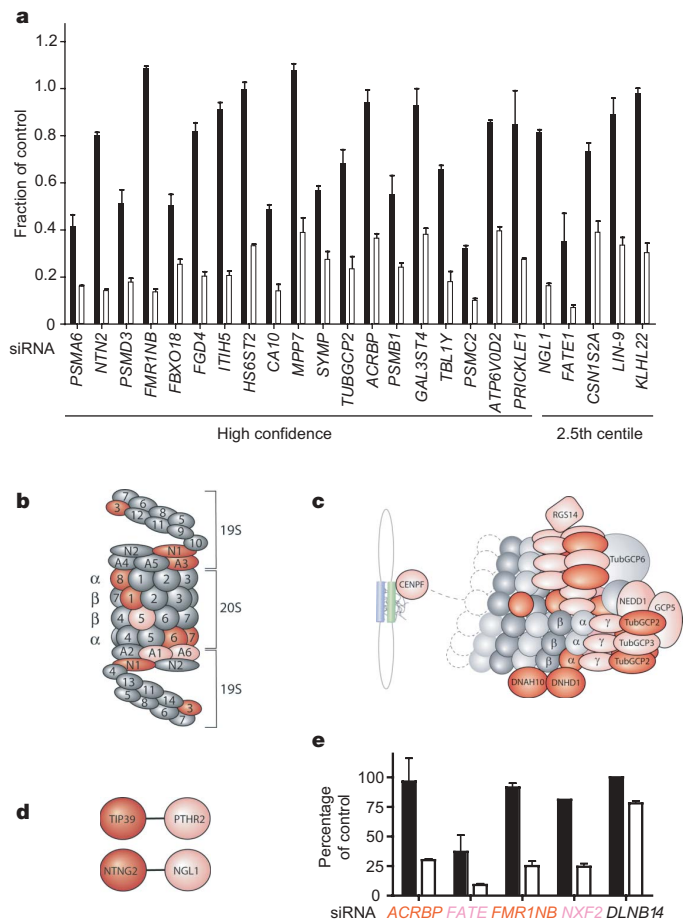

Figure 1 | Functional relationships among candidate paclitaxel-sensitizing siRNA targets. a, Retests of a panel of independently synthesized siRNA pools targeting candidate genes that modulate paclitaxel sensitivity. Results are cell viability normalized to control siRNA-transfected samples and are shown as means and s.e.m. for n = 3. Black bars, no paclitaxel; white bars, 10 nM paclitaxel. b, Proteasome. Red shading indicates satisfaction of 5% FDR, pink shading indicates satisfaction of 10% FDR. c, γ-TuRC and related components of the mitotic spindle apparatus. Shading is as in b. d, Ligand–receptor pairs. Shading is as in b. e, CT antigens. Results are viability normalized as a percentage of control siRNA transfected samples (DLNB14) and are shown as means and s.e.m. Black bars, 0 nM paclitaxel; white bars, 10 nM paclitaxel. siRNA gene shading is as in b. Values are representative of a minimum of three independent experiments.
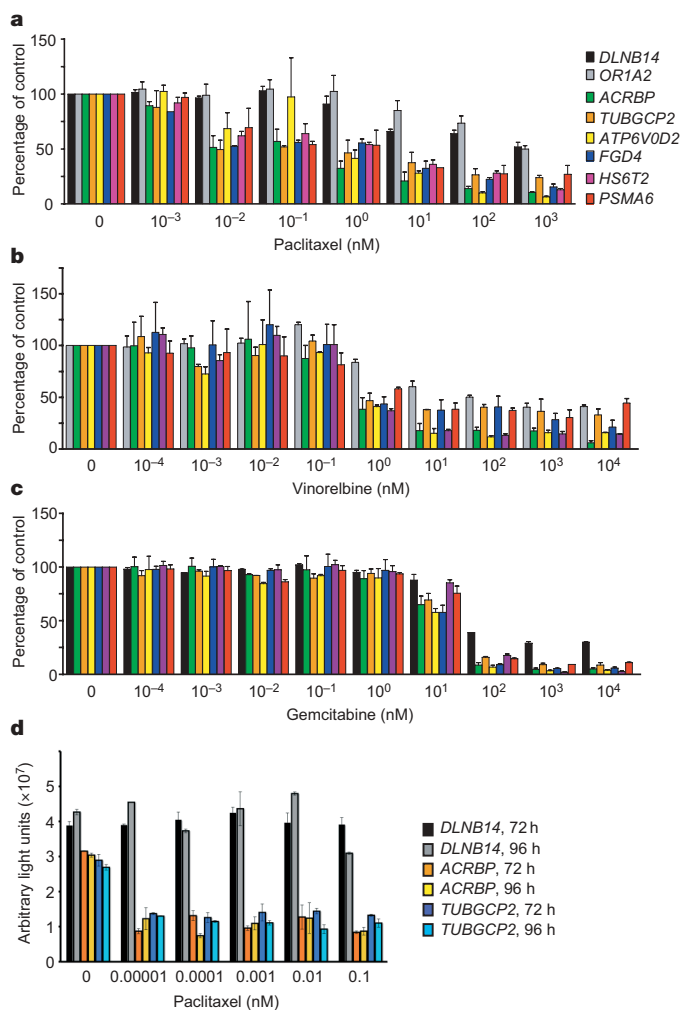
Figure 2 | Drug sensitivity profiles. a–c, H1155 transfected with siRNAs targeting the indicated genes (DLNB1 and OR1A2 are control siRNAs) were exposed to paclitaxel (a), vinorelbine (b) or gemcitabine (c) 48 h after transfection at the indicated doses for 48 h. Results are viability normalized to siRNA-transfected samples in the absence of drug and are shown as means and s.e.m. Values are representative of three independent experiments. d, H1155 transfected with siRNAs targeting the indicated genes were treated with paclitaxel 48 h after transfection for the indicated times. Bars are cell viability obtained with Cell Titer Glo and are shown as means and s.e.m.

of numerous micronucleated cells, indicating mitotic slippage through a defective spindle assembly checkpoint (Fig. 3a). Depletion of PSMA6, HS6ST2 and ATP6V0D2 did not affect mitotic spindle assembly (data not shown).

Given the significant genetic heterogeneity between cancer cell lines we next examined the effect of target depletion on a panel of lung lines, with diverse paclitaxel IC$_{50}$ values, that included the NSCLC line HCC4017 and normal, non-malignant bronchial epithelial line HBEC30 (ref. 15), isolated from the same individual. Out of 12 targets tested with the patient-matched tumour and normal lines, the depletion of 4 targets selectively sensitized the tumour-derived line to low-dose paclitaxel (Supplementary Fig. 5a). Two of the four sensitizers were in the CT-antigen family. Three out of four CT antigens tested also sensitized at least one additional NSCLC line to low-dose paclitaxel with no measurable consequences on the viability of HBEC30 cells. Not surprisingly, proteasome subunit depletion was broadly effective in tumour cells in comparison with normal cells (Supplementary Fig. 5a).

We also examined the effect of ACRBP or TubGCP2 depletion on mitotic progression in these lines. Although neither ACRBP nor TUBGCP2 depletion affected cell viability as assessed by ATP concentration in H1299 and H2126 NSCLC cells, depletion of these targets did enhance paclitaxel-induced mitotic arrest (Supplementary Fig. 5b). The lack of change in viability may reflect differences in the coupling of spindle assembly checkpoint machinery to apoptosis in different cancer cell lines[16]. Consistent with this was our observation that depleting ACRBP or TUBGCP2 sensitized H1155 cells to paclitaxel-induced caspase activation (Supplementary Fig. 5d), whereas in H2126 cells, depletion of ACRBP collaborated with paclitaxel to inhibit proliferation (Supplementary Fig. 6a). In addition, the depletion of either ACRBP or TUBGCP2 in lung-tumour-derived cell lines lacking a robust spindle assembly checkpoint (HCC366, HCC15 or HCC4017) was sufficient to induce the accumulation of non-proliferating micronucleated cells, which are normally observed after exposure to paclitaxel (Fig. 3c, and Supplementary Fig. 6b, c). These observations highlight the emerging concept that products of anomalous gene-expression programmes can become engaged to buttress the fundamental biological systems required for the proliferative fitness of cancer cells. In a specific sense, aberrant expression of proteins such as ACRBP may contribute to mitotic progression in cancer cells by enhancing the robustness of an otherwise weakened mitotic spindle apparatus.

An expected outcome of genomic chemosensitizer screens is the identification of gene products that are targets of currently available compounds, indicating novel combinatorial therapeutic regimens. Our isolation of the proteasome exemplifies this relationship because collaboration between bortezomib, a proteasome inhibitor, and paclitaxel has been demonstrated clinically[17]. Isolation of ATP6V0D2, a subunit of the vacuolar ATPase (V-ATPase)[18] (Table 1 and Fig. 1a), predicts that lysosomal ATPase-inhibitors may be effective cytocidal agents in combination with paclitaxel. Salicylihalamide A was originally identified as an anti-tumour agent and was subsequently found to target V-ATPase activity directly[19,20]. Exposure of H1155 cells to increasing doses of a synthetic salicylihalamide derivative[21], RTA 203, together with low-dose paclitaxel revealed a significant collaborative impact on viability at doses well below that required for the activity of a single agent (Fig. 3d, e). This observation highlights the strong predictive power of genome-wide synthetic-lethal screens for identification of productive drug–drug interactions. We have used a high-throughput functional-genomics screening platform, together with an objective 'hit' selection criterion derived from probabilistic judgments of error rates, to produce an unbiased and high-confidence collection of the molecular components modulating chemosensitivity in lung cancer cells. The results reveal major fulcrums of the autonomous response of cancer cells to abrogation of microtubule dynamics; the results also identify therapeutic targets for combinatorial chemotherapy and highlight a major contribution of cancer-associated anomalous gene expression patterns for support of mitotic progression in cancer cells.

Figure 3 | Convergence of paclitaxel and sensitizer gene function on mitotic spindle integrity. a, At 48 h after transfection with the indicated siRNAs, H1155 cells were exposed to the indicated paclitaxel concentrations for 24 h. Microtubules, genomic DNA and centrosomes were revealed by immunostaining with β-tubulin, 4,6-diamidino-2-phenylindole (DAPI) and α-pericentrin, respectively. Arrowheads indicate the formation of micronuclei as a consequence of bypass of MAD2-dependent mitotic spindle checkpoint arrest. Pictures are representative of a minimum of five independent experiments. Pac., paclitaxel. b, siRNA-dependent depletion of ACRBP and MAD2 was verified by immunoblots of whole-cell lysates from a. c, The interphase nuclear morphology of HCC366 cells transfected with the indicated siRNAs was examined with DAPI. Arrowheads indicate cells containing multiple micronuclei. Pictures are representative of a minimum of three independent experiments. d, Collaborative impact of paclitaxel and RTA-203 on H1155 cell viability. Results are viability normalized to untreated control samples (black bar) and are shown as means and s.e.m. Yellow bars, RTA-203 alone; blue bars, paclitaxel alone; green bars, RTA-203 plus paclitaxel at the indicated doses. Values are representative of three independent experiments. e, Percentage apoptosis as indicated by cleaved caspase-3 immunostaining of H1155 cells after a 24-h exposure to 10 nM paclitaxel or 200 nM RTA-203, or a combination of both. Error bars show s.e.m. for four independent experiments.

METHODS

All cells were reverse-transfected with siRNA pools complexed with DharmaFECT reagent (optimized for each cell type). Cells were treated 48 h after transfection and viability was assessed after an additional 48 h. For screening data analysis, each siRNA pool was assigned a viability ratio. Viability ratios were ranked by reproducibility between three replicates for each condition, using a two-sample t-test followed by a Benjamini–Hochberg correction. Immunofluorescence was performed with the use of standard fixation and permeabilization protocols. Cells were stained with monoclonal β-tubulin antibodies, polyclonal pericentrin antibodies, bromodeoxyuridine or antibodies against cleaved caspase-3 followed by secondary labelling with secondary fluorescein isothiocyanate-conjugated anti-mouse antibodies or tetramethylrhodamine β-isothiocyanate-conjugated anti-rabbit antibodies. Cells were observed under a Zeiss Axioplan 2E microscope equipped with a Hamamatsu monochrome

digital black-and-white camera and Open Lab Software. Quantitative polymerase chain reaction was performed on RNA extracted from all cells with the Roche LightCycler System or the 7900HT Fast Real-Time PCR System with primers flanking at least two siRNA target sequences and lying on separate exons. Growth inhibition assays were performed with a Sulphorhodamine B protocol on cells treated for 48 hours with the indicated drugs[22]. For colony formation assays, transfected and treated cells were replated and stained with Geimsa 5 days later. Immunoblots were performed on whole-cell lysates from H1155 cells with the use of standard protocols.

A detailed description of the screening strategy and statistical analysis is given in Supplementary Fig. 1 and Supplementary Methods. Optimized transfection protocols and growth conditions for the multiple cell lines used in this study are described in Supplementary Table 6. siRNA sequences and reverse transcriptase-mediated polymerase chain reaction primers are described in Supplementary Tables 5 and 7. Methods for standard viability assays and quantification of mitotic progression are also included in Supplementary Methods.

1. Green, D. R. & Evan, G. I. A matter of life and death. *Cancer Cell* 1, 19–30 (2002).
2. Chien, Y. & White, M. A. RAL GTPases are linchpin modulators of human tumour-cell proliferation and survival. *EMBO Rep.* 4, 800–806 (2003).
3. Matheny, S. A. *et al.* Ras regulates assembly of mitogenic signalling complexes through the effector protein IMP. *Nature* 427, 256–260 (2004).
4. Malo, N., Hanley, J. A., Cerquozzi, S., Pelletier, J. & Nadon, R. Statistical practice in high-throughput screening data analysis. *Nature Biotechnol.* 24, 167–175 (2006).
5. Benjamini, Y. H. Y. Controlling the false discovery rate: a practical and powerful approach to multiple testing. *J. R. Statist. Soc. B* 57, 2890300 (1995).
6. Allison, D. B., Cui, X., Page, G. P. & Sabripour, M. Microarray data analysis: from disarray to consolidation and consensus. *Nature Rev. Genet.* 7, 55–65 (2006).
7. Wit, E. & McClure, J. Statistical adjustment of signal censoring in gene expression experiments. *Bioinformatics* 19, 1055–1060 (2003).
8. Benjamini, Y. & Hochberg, Y. Controlling the false discovery rate: a practical and powerful approach to multiple testing. *J. R. Statist. Soc. B* 57, 289–300 (1995).
9. Jordan, M. A. & Wilson, L. The use and action of drugs in analyzing mitosis. *Methods Cell Biol.* 61, 267–295 (1999).
10. Moritz, M. & Agard, D. A. Gamma-tubulin complexes and microtubule nucleation. *Curr. Opin. Struct. Biol.* 11, 174–181 (2001).
11. Jordan, M. A. & Wilson, L. Microtubules as a target for anticancer drugs. *Nature Rev. Cancer* 4, 253–265 (2004).
12. Scanlan, M. J., Simpson, A. J. & Old, L. J. The cancer/testis genes: review, standardization, and commentary. *Cancer Immun.* 4, 1–15 (2004).
13. Toschi, L., Finocchiaro, G., Bartolini, S., Gioia, V. & Cappuzzo, F. Role of gemcitabine in cancer therapy. *Future Oncol.* 1, 7–17 (2005).
14. Weaver, B. A. & Cleveland, D. W. Decoding the links between mitosis, cancer, and chemotherapy: The mitotic checkpoint, adaptation, and cell death. *Cancer Cell* 8, 7–12 (2005).
15. Ramirez, R. D. *et al.* Immortalization of human bronchial epithelial cells in the absence of viral oncoproteins. *Cancer Res.* 64, 9027–9034 (2004).
16. Rieder, C. L. & Maiato, H. Stuck in division or passing through: what happens when cells cannot satisfy the spindle assembly checkpoint. *Dev. Cell* 7, 637–651 (2004).
17. Davies, A. M. *et al.* Bortezomib-based combinations in the treatment of non-small-cell lung cancer. *Clin. Lung Cancer* 7 (Suppl 2), S59–S63 (2005).
18. Kawasaki-Nishi, S., Nishi, T. & Forgac, M. Proton translocation driven by ATP hydrolysis in V-ATPases. *FEBS Lett.* 545, 76–85 (2003).
19. Boyd, M. R. *et al.* Discovery of a novel antitumor benzolactone enamide class that selectively inhibits mammalian vacuolar-type (H$^+$)-ATPases. *J. Pharmacol. Exp. Ther.* 297, 114–120 (2001).
20. Xie, X. S. *et al.* Salicylihalamide A inhibits the V0 sector of the V-ATPase through a mechanism distinct from bafilomycin A1. *J. Biol. Chem.* 279, 19755–19763 (2004).
21. Wu, Y., Liao, X., Wang, R., Xie, X. S. & De Brabander, J. K. Total synthesis and initial structure–function analysis of the potent V-ATPase inhibitors salicylihalamide A and related compounds. *J. Am. Chem. Soc.* 124, 3245–3253 (2002).
22. Skehan, P. *et al.* New colorimetric cytotoxicity assay for anticancer-drug screening. *J. Natl Cancer Inst.* 82, 1107–1112 (1990).

Supplemental Figure 1: Genome-wide chemosensitization screen. A. Efficient protein depletion under conditions of high-throughput siRNA transfection of H1155 was validated by immunoblot analysis of the indicated proteins from whole cell lysates. B. Workflow for the primary triplicate two-condition analysis. C. A sample of 5 paclitaxel dose-response curves from daily control plates produced during the primary screen. Values represent viability normalized to untreated samples. D. Frequency distribution of viability ratios (survival in paclitaxel/survival in carrier) resulting from each of 21,127 siRNA pools. E. Schematic of the protocol derived to define high confidence paclitaxel-sensitizing targets:

Data processing and analysis procedure

A blinded data analyst carried out data processing and analysis independently of gene annotations. The following steps were performed:

1. Each measurement of a specific well was first normalized by plate reference well (measurement of each experimental well was divided by the reference well of the plate). The biological replicates (three for each condition) were averaged (Average$_{paclitaxel}$, Average$_{carrier}$; Supplemental Table 1).
2. For each gene, a two sample t-test (with pooled variance) was performed, using standard operations in GeneSpring and SAS, to determine whether there was a significant difference between the averaged values under the two experimental conditions. A P-value was then recorded (Supplemental Table 1).
3. With the 20,960 P-values generated in step 2, Benjamini-Hochberg's method to control the false discovery rate (FDR) was performed [5-7], again using standard operations in GeneSpring and SAS. The essence of this method is to inflate the raw *p*-values based on their rank in the distribution of all the P-values. Let $P_{(i)}$ = the *p*-value of gene *i*, let *i* = rank of $P_{(i)}$ in the distribution, let *m* = total number of comparisons (i.e. genes in the genome, in our case, *m*=20,960) and let *q** = false discovery rate, the FDR for the ith gene FDR(*i*)= $P_{(i)}$ (*m*/*i*). Since we pre-specified the FDR criterion as FDR≤0.05, genes with a FDR less or equal to 0.05 were selected (Supplemental Table 2).
4. In order to take the magnitude of response into account, the 20,960 viability ratios (Average$_{paclitaxel}$/Average$_{carrier}$; Supplemental Table 1) were sorted in ascending order and the genes with a fold change among the lowest 2.5 percentile of the fold change distribution were selected (Supplemental Table 3). Genes that were identified by both step 3 (FDR≤0.05) and step 4 (fold change among the lowest 2.5%) were included in the high priority hit list for further validation and functional tests (Table 1).

F. Frequency distribution for carrier and paclitaxel treated cells transfected with 21,127 genes.

Supplementary Figure 2. A. qPCR analysis of gene expression in H1155 cells transfected with indicated siRNAs pools. Error bars represent standard deviation among replicates. Values are representative of a minimum of 2 independent experiments performed in duplicate. B. Individual siRNAs versus pools. Each of the 4 unique siRNAs present in the siRNA pools targeting the indicated genes were retested individually to examine consequences on H1155 paclitaxel responsiveness. Black bars (0 nm paclitaxel), white bars (10 nM paclitaxel) +/- SEM. C. As in A, except distinct pools of four more independent siRNAs were used. D. As described in A, except distinct pools of four more independent siRNAs against each gene (hit pool #2) were used. DLNB14 siRNA as in A.

Supplementary Figure 3. A. Percentage of cells remaining following gene silencing and paclitaxel treatment. H1155s were transfected with indicated siRNAs and treated with indicated doses of paclitaxel 48 hours post transfection. Cells were counted 48 hours post drug treatment. Lower panel indicates growth curve for untreated cells transfected with control siRNA. Error bars represent standard error from the mean. Values are representative of 2 independent experiments performed in duplicate B. Colony formation assay in H1155 cells following gene silencing and paclitaxel treatment. Cells were treated as in A followed by replating for 8 days. Values are standard error from the mean for 2 independent experiments.

Supplementary Figure 4. FGD4 depletion induces accumulation of mitotic figures. A. 72 hours post siRNA-transfection, cells were fixed and stained with β–Tubulin and DAPI. Mitotic figures were scored microscopically and are expressed as a percentage of total cell number examined.

Error bars indicate standard deviation from the mean from 4 independent experiments. OR1A2 siRNAs were used as a negative control.

Supplementary Figure 5. Impact of siRNA on taxol sensitivity among multiple human lung cell lines. A. siRNAs targeting the indicated genes were transfected into the indicated cell lines. 48 hours post transfection cells were treated with cell line specific paclitaxel doses that were determined to be at least 10 fold lower than otherwise sufficient to engage a response. Cells were treated as follows: 0.1 nM paclitaxel (HCC1193, HCC4017), 1.0 nM paclitaxel (H2126, H1299) or 10 nM paclitaxel (HBEC30) for 48 (H2126, HCC4017, HBEC30) or 72 (HCC1193, H1299) hours. The additional 24 hour paclitaxel exposure for HCC1193 and H1299 was required to engage apoptosis with higher paclitaxel concentrations. For comparison, HBEC30 viability is unchanged by an additional 24 hour exposure (data not shown). B. Impact of depletion of indicated genes on accumulation of mitotic figures in multiple lung cell lines. Cells were assayed 24 hours post paclitaxel treatment. H1299 and H2126s were treated with 1 nM paclitaxel. H1155s and HBEC30s were treated with 10 nM paclitaxel. Error bars are standard error from the mean. Values are representative of a minimum of 2 independent experiments performed in duplicate. C. Dose response analysis in HBEC30s that identifies 100nM paclitaxel as minimally sufficient to induce aberrant mitosis in these cells. Error bars are standard error from the mean for 3 independent experiments. Right hand panel is qPCR indicating depletion of TUBGCP2 in HBEC30s. D. Cleaved caspase-3 expression in H1155 cells transfected with indicated siRNAs and treated with paclitaxel for 48 hours at indicated concentrations.

Supplementary Figure 6. Impact of hit depletion on cellular phenotypes. A. % of BrdU positive H2126 cells transfected with indicated siRNAs. 48 hours post transfection, H2126s were treated with paclitaxel for 24 hours. Error bars are standard error from the mean for 2 independent experiments performed in duplicate. B. Accumulation of aberrant tetraploid nuclei (micronucleated) in cell lines transfected with indicated siRNAs and treated for 24 hours. HCC15s were treated with 0.1 nM paclitaxel. HCC4017 were treated with 1 nM paclitaxel. HCC366s were treated with 100 nM paclitaxel. Error bars represent standard error from the mean for 3 independent experiments. C. % of BrdU positive HCC366 cells transfected with indicated siRNAs. Cells were assayed 72 hours post transfection (no paclitaxel). Error bars represent standard error from the mean for 2 independent experiments.

Description of Supplementary Tables:

Supplemental Table 1: Full data set containing mean, S.D., p-values, and associated gene annotations from the genome-wide screen.

Supplemental Table 2: 5% FDR gene list.

Supplemental Table 3: 2.5 percentile gene list.

Supplemental Table 4: *p*-values and FDR values for genes described in Figure 2.

Supplemental Table 5: siRNA sequences corresponding to the HC hit list.

Supplemental Table 6: Transfection conditions for all cell lines used in this study.

Supplemental Table 7: Primer sequences used for quantitative rtPCR.

Supplemental Methods

Cells and Reagents: The cancer cell lines used are all of NSCLC origin: NCI-H1155 (lymph node metastasis), HCC366 (primary tumor), HCC193 (pleural effusion), NCI-H1299 (lymph

node metastasis), HCC15 (lymph node metastasis), HCC4017 (primary tumor), and were

maintained in RPMI (Gibco) + 5 % FBS (Atlanta Biologicals) and 1X Antibiotic/Anitmycotic

(Gemini) . Non-tumorigenic human bronchial epithelial cells, HBEC3-KT, HBEC30-KT and

HBEC34-KT, were derived from histologically normal bronchus as described[22]. HCC4017 and

HBEC30-KT were derived from the same patient. Paclitaxel was purchased from Sigma.

Vinorelbine (Sicor Pharmaceuticals) and Gemzar (Gemcitabine HCl, Eli Lilly) were purchased

from the UTSW pharmacy. A genome-wide synthetic siRNA library (Dharmacon set # G-

005000-01), corresponding to all unique genes present in the human RefSeq database V5.0, was

arrayed in columns 2-11 on 96-well microtiter plates. Each well contained a 2 nmole mixture of

4 different synthetic siRNA duplexes against a single gene target. We compiled gene

annotations for each siRNA pool from the SOURCE (http://genome-www5.stanford.edu/cgi-

bin/source/sourceSearch) and UCSC genome browser (http://genome.ucsc.edu/index.html)

databases and incorporated these into a single Microsoft Excel file (Supplementary Table 1).

The annotations include array location, barcode, target gene ontology, target gene chromosomal

location, target gene names and aliases, target gene accession number, target gene Unigene

number, and target gene LocusLink number. SiRNA sequences used to target the 87 genes

identified as high-confidence paclitaxel-sensitizer genes are listed in supplementary Table 4.

Antibodies: MAD2 (Medical and Biological Laboratory), ERK1/2 (Santa Cruz), CDK2 (Santa

Cruz), E-Cadherin (BD Transduction Labs), RalA (BD Transduction Labs), Cleaved caspase-3

(Cell Signalling). Anti-sp32 (ACRBP) was a kind gift from Janice Bailey.

Transfection Protocol: For high throughput transfection, 8 pmoles of each siRNA pool in a

volume of 30 ul of RPMI was delivered to each of 6 assay plates/ master plate using a Biomek

FX robotic liquid handler (Beckman Coulter). 0.4 ul of Dharmafect 1 (Dharmacon) in 9.6 ul of

RPMI was then delivered to each well using a TiterTek Multidrop. Following a 20 -30 minute incubation, 1×10^4 NCI-H1155 cells from a trypsin-mediated single-cell suspension were delivered to the siRNA/liposome complexes in a total volume of 200 ul. Plates were incubated for 48 hours at 37°C/5% CO_2 after which a Hydra 96 (Robbins-Scientific) was used to removed 150 ul of the medium. 50 ul of fresh media or fresh media+20 nM paclitaxel in media was then delivered by Multidrop. Following an additional 48 hours incubation at 37°C/5% CO_2, 15 ul of Cell-Titer Glo Reagent (CTG) (Promega) was delivered to each well and incubated according to manufacturer protocol. Luminescence was recorded using an Envision Plate Reader (Perkin Elmer). All other transfection conditions were as described in Supplemental Table 6.

Statistical Analysis: Raw luminescence values collected from the high throuput screen were normalized to internal reference control samples (cells with no siRNA in wells A1-A8) on each plate to allow for plate-to-plate comparisons. Each siRNA pool was then assigned a viability ratio corresponding to mean viability in the presence of paclitaxel over mean viability in the absence of paclitaxel. Viability ratios were ranked by reproducibility among 3 replicates for each condition using a standard two-sample t-test followed by a Benjamini/Hochberg correction for multiplicity of testing[23]. Briefly, the later is an inflation of raw *p*-values based on their rank in the distribution- where the null hypothesis is rejected if $P_{(i)} \leq (i/m)q^*$ (let $P_{(i)}$ = the *p*-value of gene *i*, let *i* = rank of $P_{(i)}$ in the distribution, let *m* = total number of comparisons (i.e. genes in the genome) and let q^* = false discovery rate). FDR values (false discovery rate) were therefore calculated as FDR(*i*)= $P_{(i)}$ (*m/i*). *P*-values for significance of enrichment of hits with related function were calculated by hypergeometric distribution using SAS.

Immunofluorescence: Lung cancer cells were reverse transfected onto glass coverslips in 24-well dishes (see Supplementary Table 6 for cell numbers and transfection reagent). 4.2 x10^5 HBEC cells were plated on glass coverslips in 35 mm^2 dishes and forward transfected with 100 nM siRNA using Oligofectamine (Invitrogen) according to manufacturer's protocol. All cells were incubated for 48 hours at 37°C/5%CO$_2$. Media was then removed and replaced with fresh media with or without paclitaxel. Following an additional 24 hour incubation at 37°C/5%CO$_2$, cells were fixed in 3.7 % Formaldehyde for a minimum of 15 minutes. Following 2 washes with 1x PBS, cells were permeabilized in 0.5 % TX-100 for 10 minutes and blocked in 1X PBS with 5 % BSA and 0.1 % Tween-20 (PBTA) for a minimum of 15 minutes. Coverslips were then incubated with a 1:100 dilution of monoclonal β-tubulin (Sigma), and either a 1:200 dilution rabbit polyclonal pericentrin (Abcam) or cleaved-caspase-3 (Cell Signaling) followed by extensive washing and incubation with a 1:100 dilution of FITC-anti-mouse, TRITC anti-rabbit (Jackson Immunoresearch) or 1:1000 dilution of Alexa-Fluor 594 and 488 (Invitrogen). Following 3 washes with PBTA, cells were mounted using a DAPI mounting medium (Vector Labs). For BrdU staining, cells were treated with 40 nM BrdU for 8 hours prior to fixing in 3.7 % HCHO. Cells were then permeabilized with acetone at -20°C for 5 minutes. DNA was denatured using 10 N HCl for 10 minutes. Cells were blocked in PBTA for a minimum of 10 minutes followed by incubation with a 1:40 dilution of Alexa-Fluor-488-FITC for 1 hour at room temperature. Following 3 washes with PBTA, cells were mounted as described above. Cells were visualized using an Axioplan 2E microscope (Carl Zeiss) equipped with a Hamamatsu monochrome digital black and white camera and Open Lab Software (Improvision).

qPCR: 6 x 10^5 NCI-H1155 cells were transfected in 35 mm^2 dishes with 50 nM siRNA. HBEC cells were transfected as described above. RNA was extracted from all cells with High Pure

RNA Isolation Kit (Roche Applied Science) according to the manufacturer's protocol 72-96 hours post-transfection. cDNA was sythesized with Super Script II Reverse Transcriptase (Invitrogen) according to the manufaturer's protocol. For cDNA synthesis of most genes, 1 ug of RNA and oligo(dT)$_{12-18}$ primers were used with the exception of ATP6V0D2, which required 5 ug of RNA. One fifteenth of the cDNA reaction was used with either the Roche LightCycler System and the Light Cycler FastStart DNA Master SYBR Green I (Roche Applied Systems) or the 7900HT Fast Real-Time PCR System and the SYBR Green PCR Master Mix (Applied Biosystems). Primers were chosen to flank at least two siRNA target sequences and lie on separate exons when possible. Values were normalized using GAPDH and analyzed using the relative quantification mathematical model (Pfaffl).

Growth inhibition assay: NCI-H1155 cells were seeded at a density of 5 x 10^3 cells/well in 96-well flat-bottom plates. Twenty-four hours later, the indicated concentrations of RTA 203 and paclitaxel were added to each well, with each combination replicated twelve times. Forty-eight hours post-treatment, cells were fixed and stained as previously described [24]. Briefly, cells were fixed with 0.1% (w/v) trichloroacetic acid at 4°C for 1 hour, washed with tap water five times and allowed to dry overnight. Dried cells were stained with 0.4% (w/v) sulfarhodamine B dissolved in 1% acetic acid for twenty minutes. Wells were washed five times with 1% acetic acid, allowed to dry, and dye was solubilized in 200 µL 10 mM Tris-base. Absorbance was read at 492 nm and growth inhibition relative to vehicle-treated cells was determined.

Supplementary Figure 1

a

b

c

d
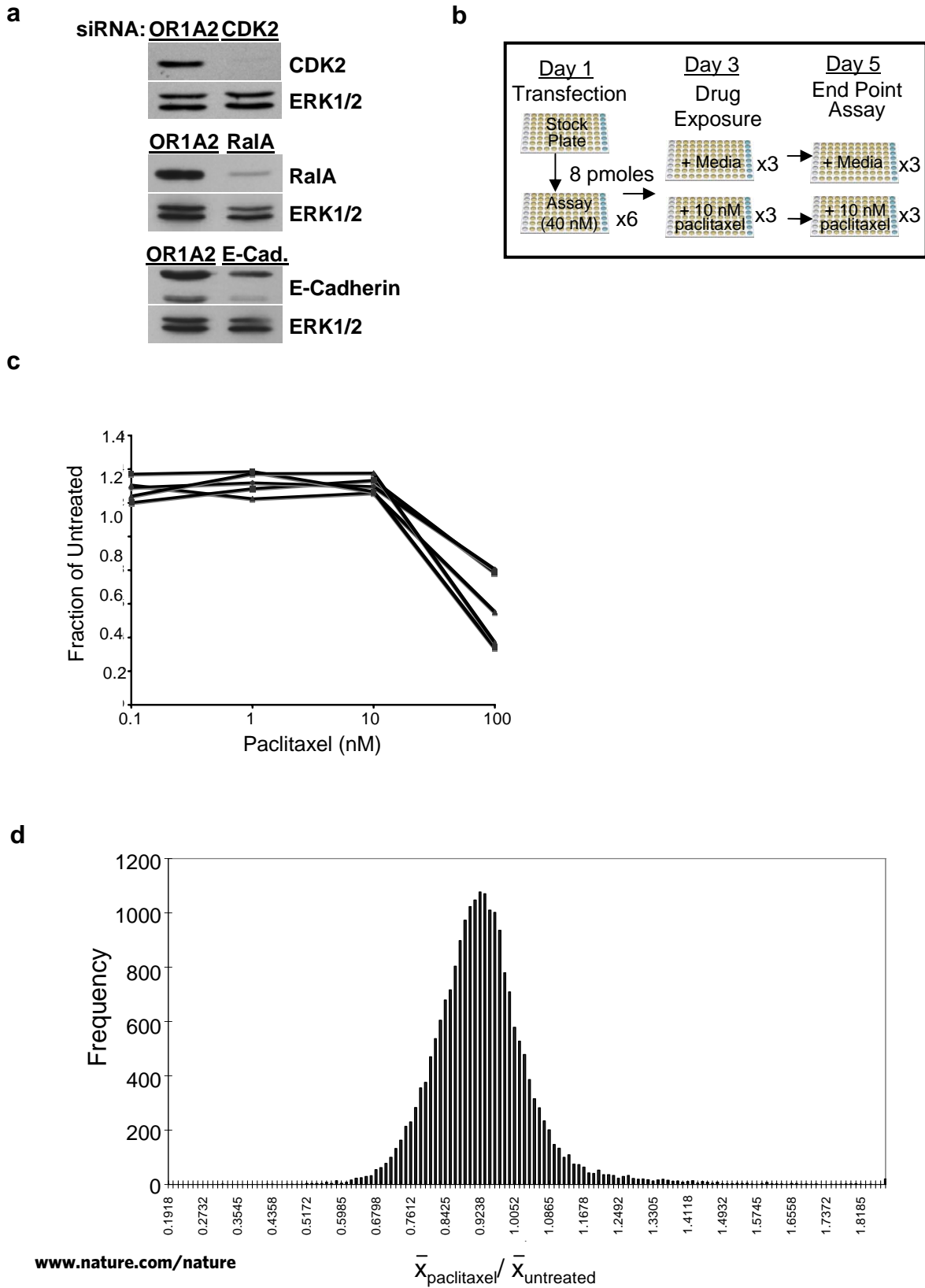
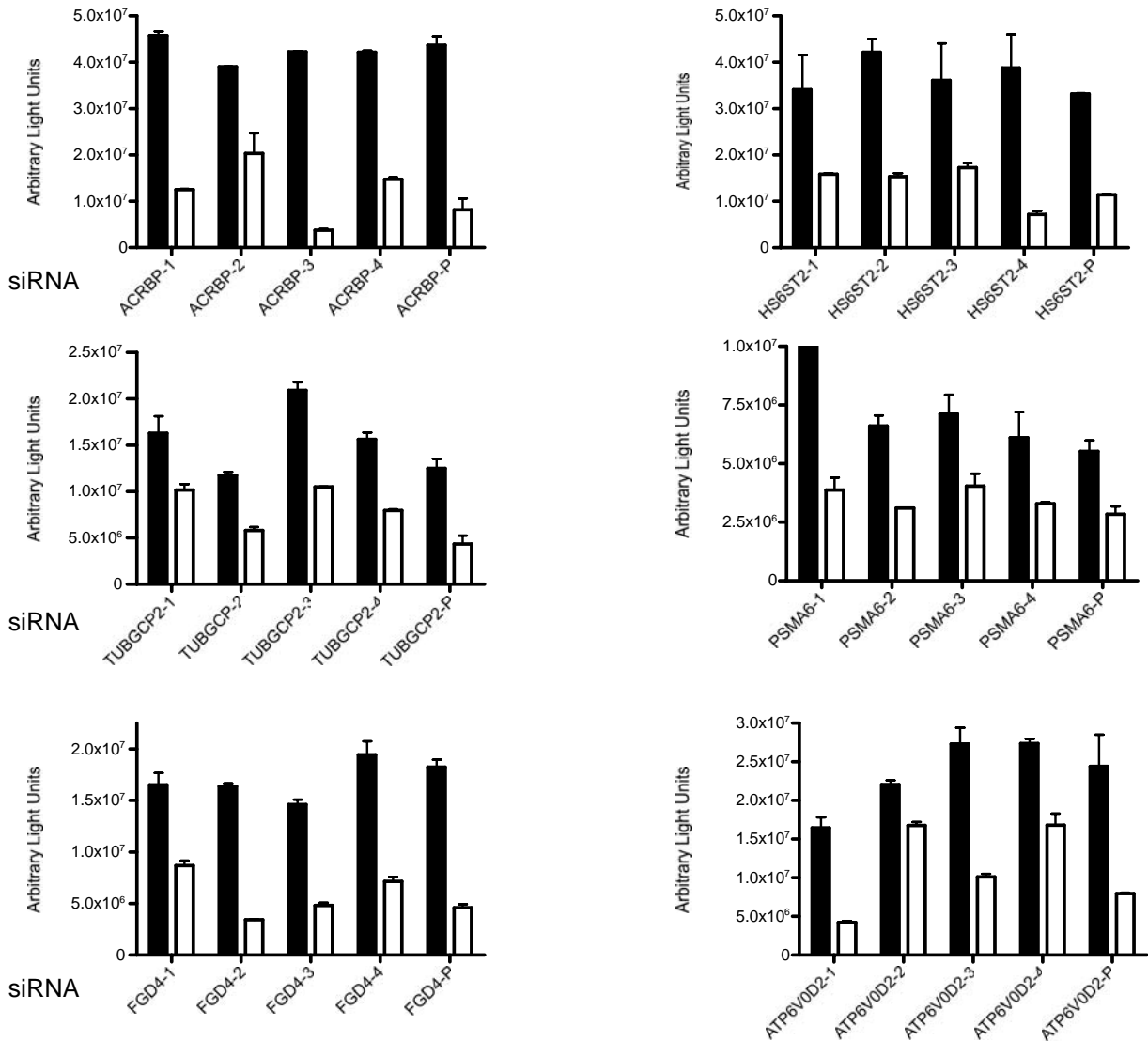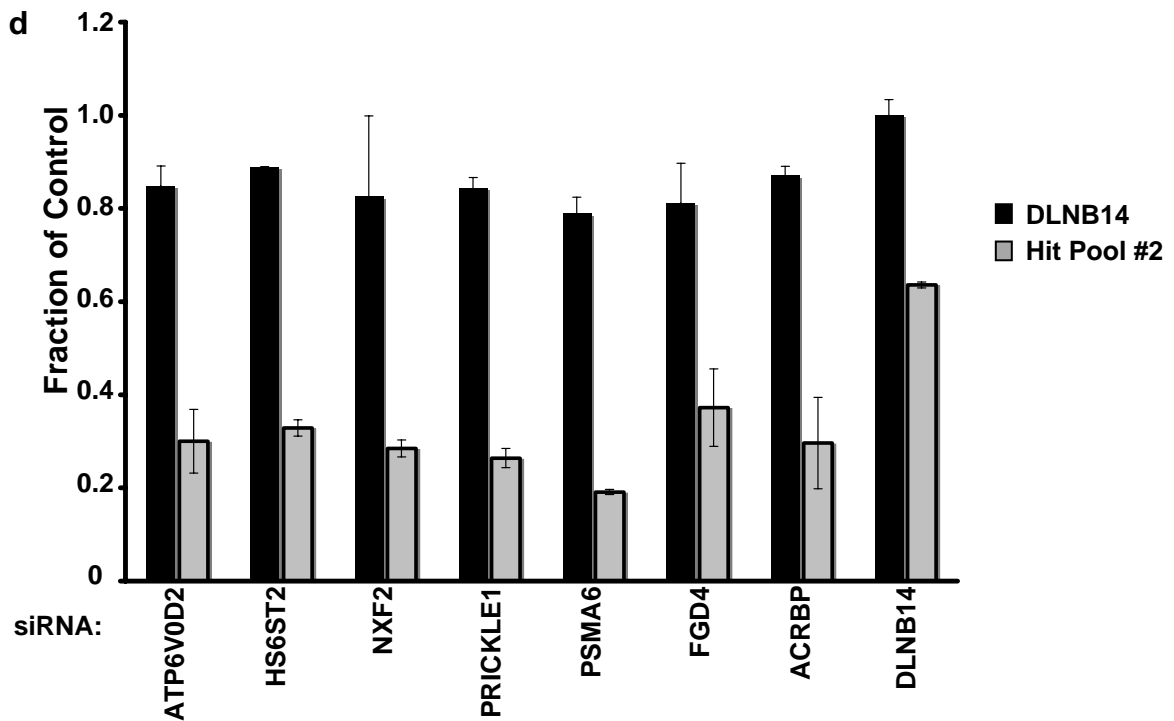## Supplementary Figure 1

e

f

Carrier   10nM paclitaxel

a
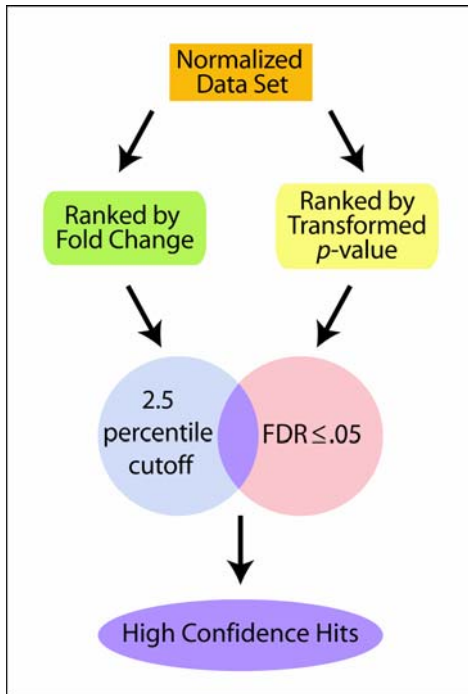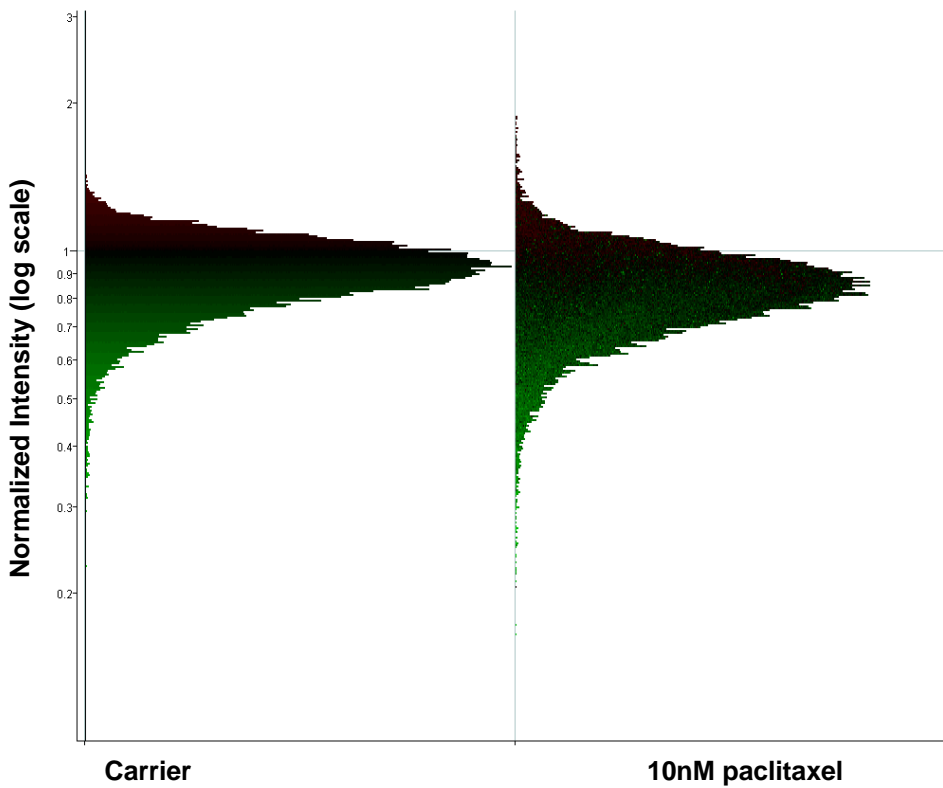
Supplementary Figure 2

b
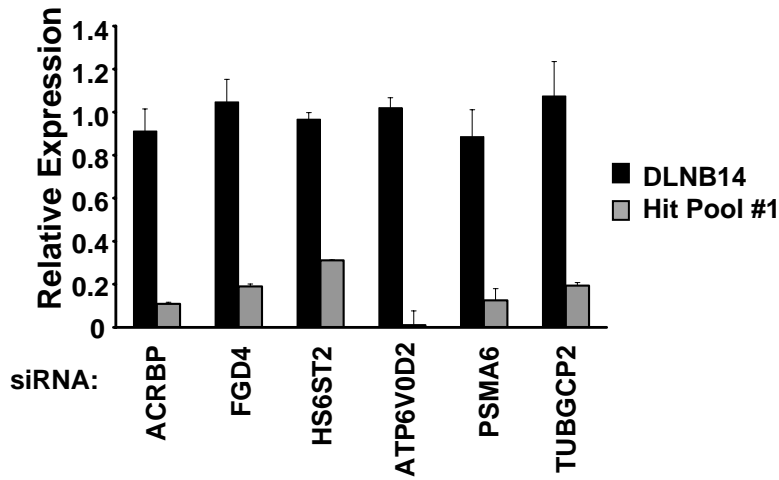
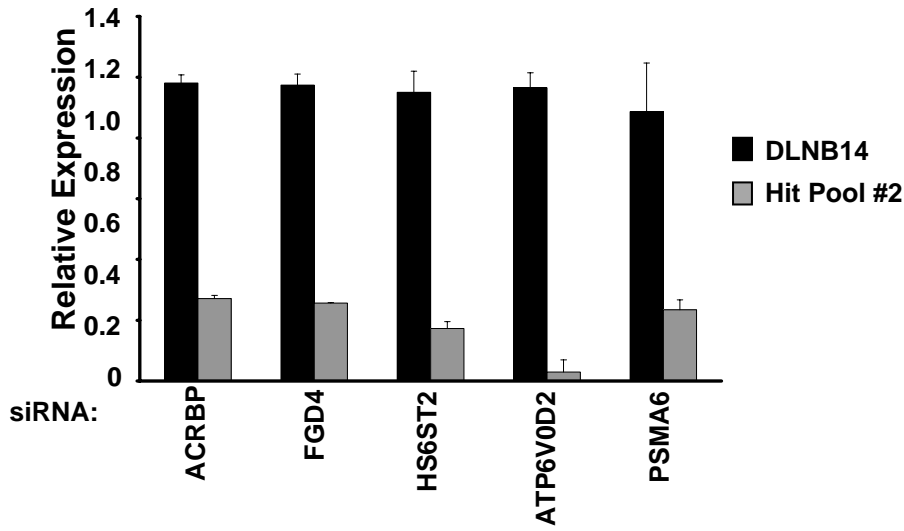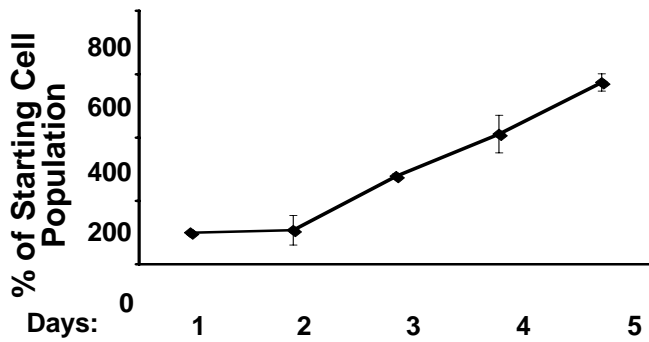## Supplementary Figure 2

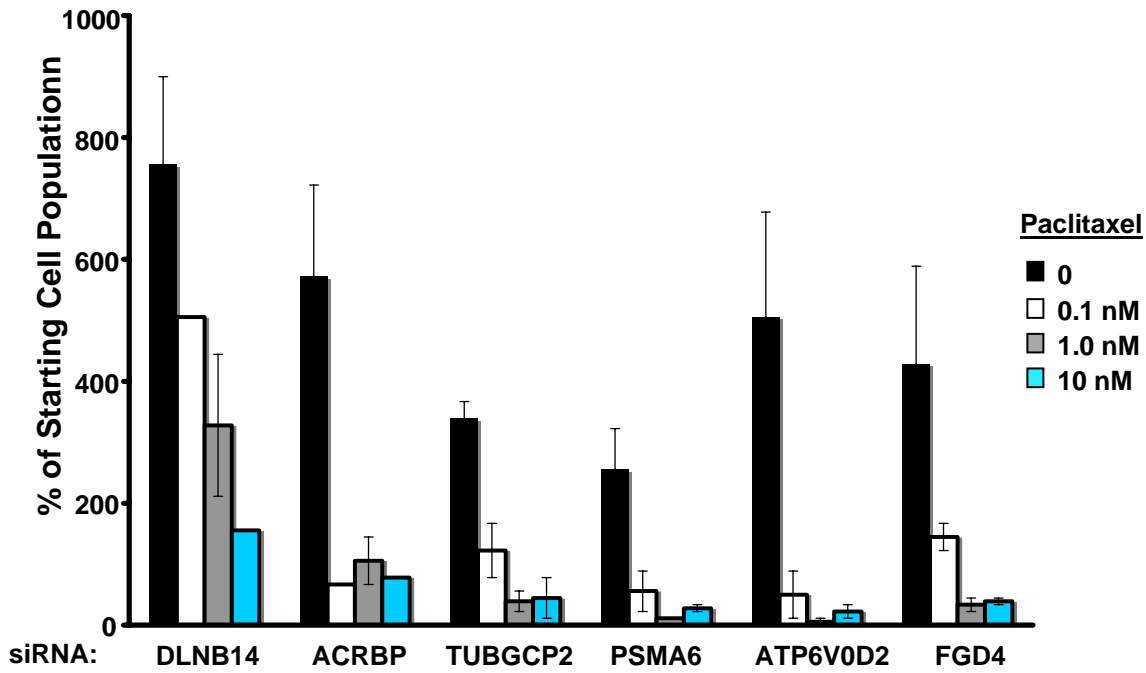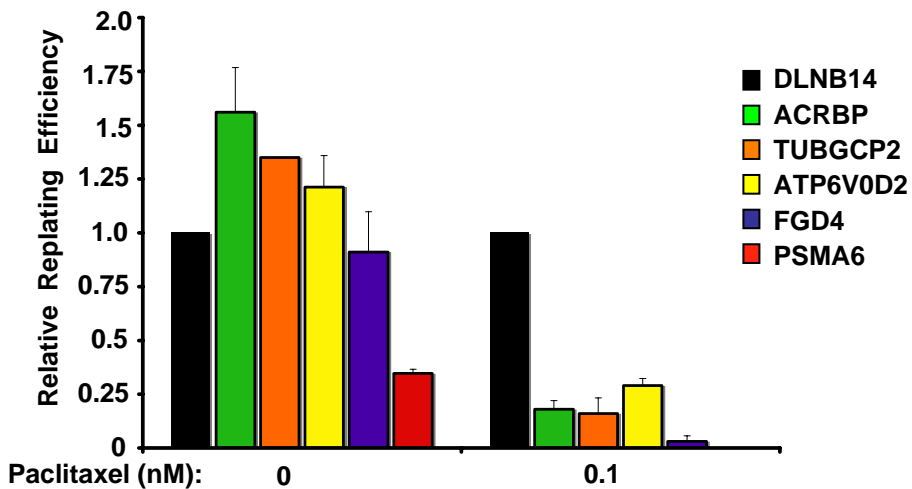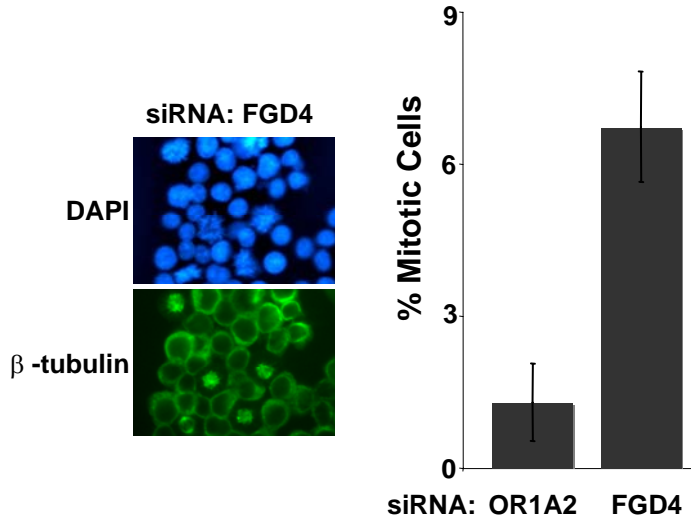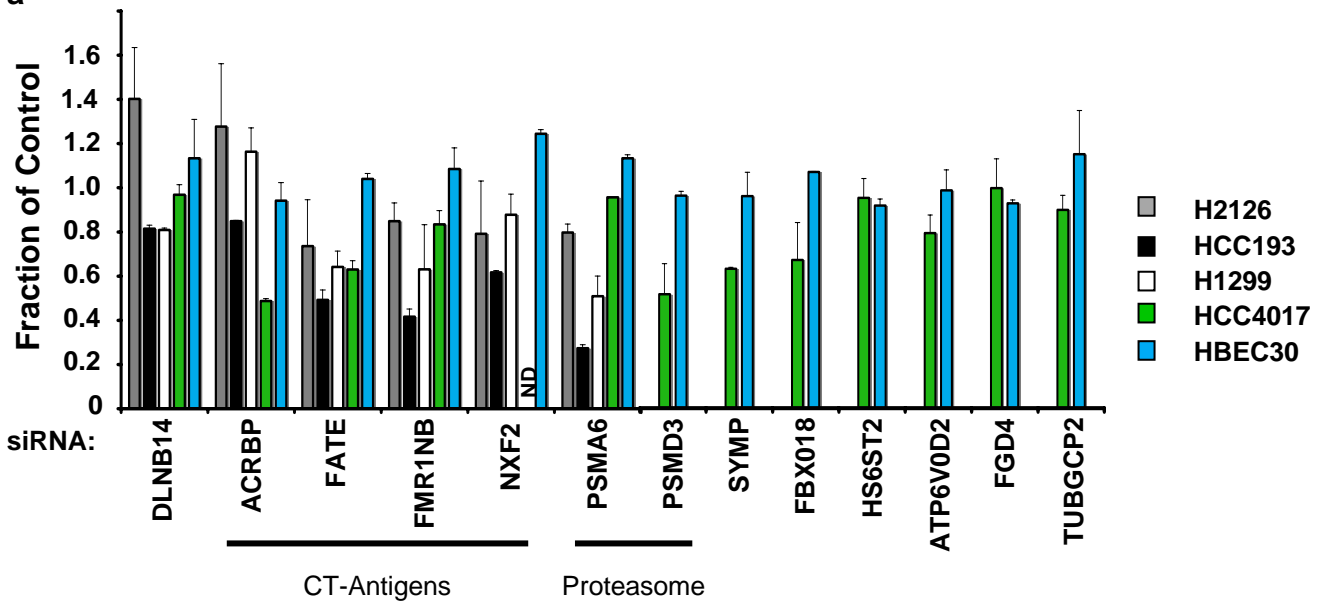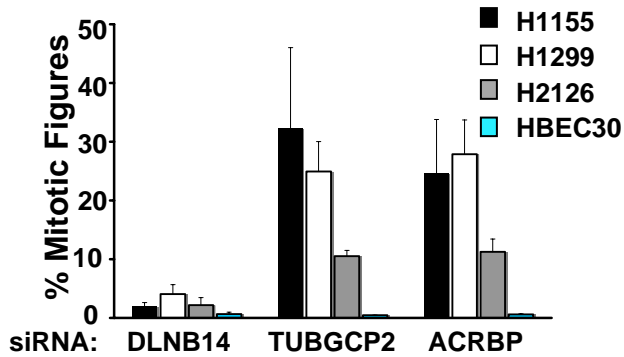Supplementary Figure 6

a

b

Supplementary Figure 4

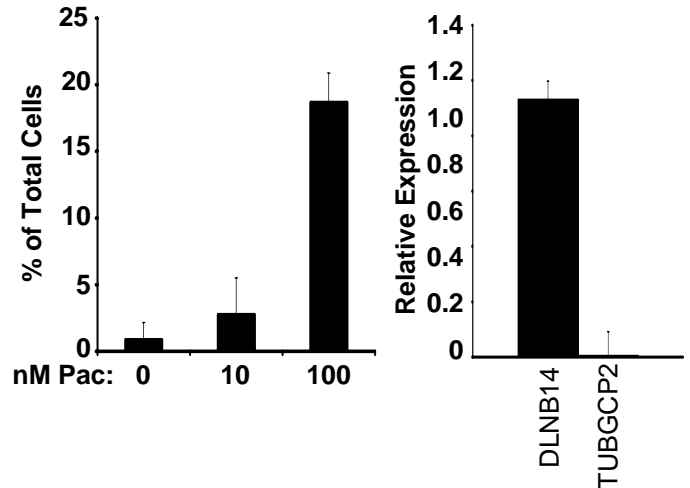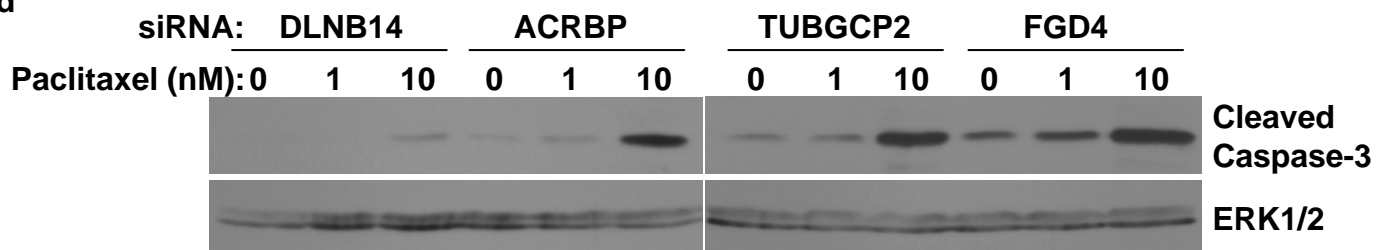## Supplementary Figure 5

Supplementary Figure 6